Molecular Cell, Vol. 4, 97–107, July, 1999, Copyright ©1999 by Cell Press

NSF N-Terminal Domain Crystal Structure: Models of NSF Function

Richard C. Yu,* Reinhard Jahn,† and Axel T. Brunger*‡
*The Howard Hughes Medical Institute and
Department of Molecular Biophysics
and Biochemistry
Yale University
New Haven, Connecticut 06520
†Department of Neurobiology
Max-Planck-Institute for Biophysical Chemistry
D-37077 Göttingen
Germany

Summary

N-ethylmaleimide-sensitive factor (NSF) is a hexameric ATPase essential for eukaryotic vesicle fusion. Along with SNAP proteins, it disassembles *cis*-SNARE complexes upon ATP hydrolysis, preparing SNAREs for *trans* complex formation. We have determined the crystal structure of the N-terminal domain of NSF (N) to 1.9 Å resolution. N contains two subdomains which form a groove that is a likely SNAP interaction site. Unexpectedly, both N subdomains are structurally similar to domains in EF-Tu. Based on this similarity, we propose a model for a large conformational change in NSF that drives SNARE complex disassembly.

Introduction

N-ethylmaleimide-sensitive factor (NSF), a member of the ATPases associated with diverse cellular activities (AAA) superfamily (Patel and Latterich, 1993; Confalonieri and Duguet, 1995), is involved in many eukaryotic membrane fusion pathways, from intra-Golgi transport to synaptic vesicle exocytosis (Bennett and Scheller, 1993; Ferro-Novick and Jahn, 1994; Rothman, 1996). These fusion events require SNAREs (SNAP receptors), membrane proteins whose cytosolic portions associate to form stable complexes, promoting and possibly driving the fusion event (Hay and Scheller, 1997; Weber et al., 1998). NSF, in an ATP hydrolysis–dependent manner, primes membranes for fusion by disrupting *cis* complexes of SNAREs, freeing them for recycling and activating them for formation of intermembrane *trans* complexes. These disassembly events require the cofactor soluble NSF attachment protein (SNAP) to bind to the SNAREs, providing a binding site for NSF (Whiteheart et al., 1992; Wilson et al., 1992). SNAP/SNARE binding stimulates NSF's ATP hydrolysis rate, and this stimulation is coincident with complex disassembly (Morgan et al., 1994; Barnard et al., 1997). In detergent-solubilized cell and tissue extracts (Wilson et al., 1992; Hayashi et al., 1994) and in vitro (Söllner et al., 1993; Hayashi et al., 1995), a distinct complex of SNAREs, α-SNAP (a specific isoform of the SNAP family), and NSF can be isolated in the presence of nonhydrolyzable ATP analogs. This 20S particle, named for its sedimentation characteristics, likely represents an intermediate in the NSF-mediated SNARE complex disassembly pathway.

NSF is a hexamer (Fleming et al., 1998; Lenzen et al., 1998; Yu et al., 1998), and only the oligomeric form is competent for SNARE complex disassembly (Whiteheart et al., 1994; Nagiec et al., 1995). Each NSF protomer consists of three domains, defined by limited proteolysis: N (residues 1–205), D1 (206–477), and D2 (478–744) (Tayaga et al., 1993). Domain deletion and swapping show that N is necessary, but not sufficient, for the binding and disassembly activities of NSF (Nagiec et al., 1995). D1 and D2 each contain an AAA cassette, a consensus sequence of around 230 amino acids characteristic of AAA proteins (Confalonieri and Duguet, 1995). This cassette includes common nucleotide-binding motifs, such as the Walker A and B boxes (Walker et al., 1982), and additional characteristic regions (Beyer, 1997). ATP binding and hydrolysis by D1 are necessary for the SNARE disassembly reaction to occur, and ATP binding, but not hydrolysis, by D2 is necessary for hexamer formation (Sumida et al., 1994; Whiteheart et al., 1994).

In electron microscopy (EM) studies, the NSF hexamer in the presence of ADP appears as a stack of two rings, corresponding to the D1 and D2 domains, respectively, which is ~10 nm high and ~13 nm wide with an ~2.5 nm diameter pore along the symmetry axis (Hanson et al., 1997; Hohl et al., 1998). The shape of the hexamer depends on the nucleotide bound to D1 (Figure 7B). In the presence of ATP-EDTA or nonhydrolyzable ATP analog, the ~10 nm long × ~13 nm wide D1-D2 rings show diffuse additional features, probably N domains, flared outward away from the pore (Hanson et al., 1997). In this ATP-bound conformation, NSF can bind the SNAP/SNARE complex. The ADP-bound morphology is slightly wider, with the D1 ring dilated to ~16 nm (Hanson et al., 1997), and does not possess outwardly flared N domains.

A coherent picture of the NSF/SNAP/SNARE interactions is beginning to emerge based on crystallographic, biochemical, and EM studies. Crystal structures of a yeast homolog of α-SNAP (Rice and Brunger, 1999 [this issue of *Molecular Cell*]) and of the core of the synaptic SNARE complex (Sutton et al., 1998) have been determined. α-SNAP consists of an N-terminal twisted sheet of helix-loop-helix repeats, followed by a globular, α-helical bundle, and the core SNARE complex is a long, all-parallel four-helix bundle. Three α-SNAPs bind to the SNARE complex (Hayashi et al., 1995) in a lateral fashion, with the N terminus of each α-SNAP close to the membrane-proximal C termini of the SNAREs (Hohl et al., 1998). NSF then binds to the SNAP/SNARE complex at the C-terminal region of α-SNAP (Barnard et al., 1996). This region of α-SNAP includes a conserved leucine residue, Leu-294, which is crucial for both stimulation of NSF ATPase activity and efficient SNARE complex disassembly (Barnard et al., 1997). In the 20S complex,

‡To whom correspondence should be addressed (e-mail: brunger@laplace.csb.yale.edu).

Table 1. Proteins Structurally Similar to N

N_A DALI[a] Structural Similarity Search Hits (Z ≥ 3.0)

Protein	Double-ψ β Barrel?	Z	C_α Rmsd (Å)
DMSO reductase	Y	5.8	2.6
1-aspartate-alpha-decarboxylase	Y	5.7	2.3
Formate dehydrogenase	Y	5.6	2.3
Barwin, basic barley seed protein	Y	4.0	2.8
1-fucose isomerase	Y	3.9	2.9
EIAV protease	Y	3.2	2.2
Phthalate dioxygenase	N	3.0	3.8
Flavodoxin reductase	N	3.0	4.1
Elongation factor Tu	N	3.0	2.9

N_B DALI[a] Structural Similarity Search Hits (All)

Protein	Z	C_α Rmsd (Å)
Elongation factor tu	2.9	3.2

NSF/EF-Tu Alignments[a]

N_A	EF-Tu[b] Domain 2
Met-1 to Cys-11	Pro-220 to Thr-230
Thr-13 to Ser-17	Ile-231 to Gly-235
Asp-28 to Ser-54	Lys-246 to Met-272
Val-56 to Ser-59	Asp-284 to Gly-287
Gln-66 to Trp-69	Ser-294 to Glu-297
Gln-76 to Ser-84	Arg-300 to Gly-308
N_B	EF-Tu Domain 3
Lys-89 to Ile-107	Ile-310 to Gly-328
Ser-109 to Met-117	His-331 to Arg-339
Phe-121 to Gln-124	Asp-348 to Gly-351
Asn-126 to Asn-141	Lys-376 to Gly-391
Asp-142 to Ala-154	Arg-393 to Glu-405

[a] Aligned strands and C_α rmsd values determined by DALI (Holm and Sander, 1993). Z is defined as the number of standard deviations above expected for similarity between the aligned protein strands.
[b] The EF-Tu PDB accession code is 1EFT.

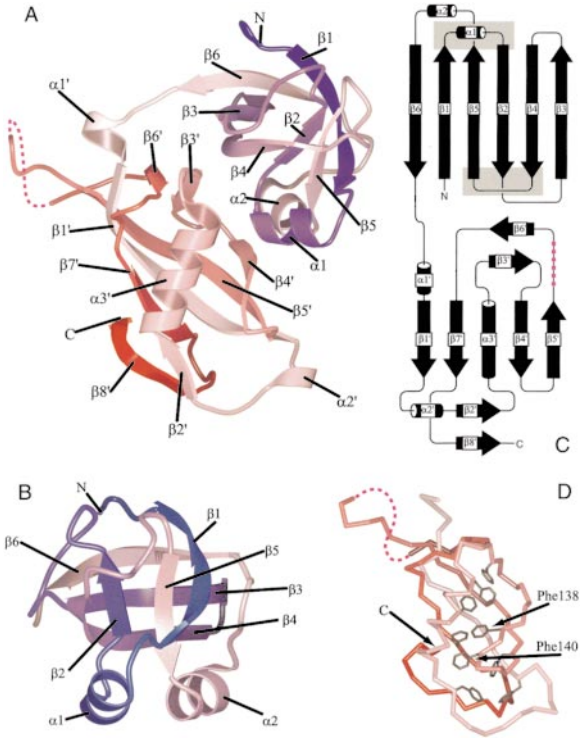

Figure 1. Secondary Structure and Topology of N

The red dashed line indicates disordered residues 162–166.
(A) Ribbon diagram rendering of N. Secondary structure was assigned using DSSP (Kabsch and Sander, 1983). The two distinct subdomains of N are referred to as N_A (residues 1–84, blue to pink) and N_B (residues 87–201), pink to red.
(B) Ribbon diagram of N_A from another perspective.
(C) Topology diagram for N_A. Shaded regions indicate the ψ loops.
(D) Aromatic ladder consisting of phenylalanine and tyrosine residues lining helix α3′ in N_B.

the NSF hexamer appears to envelop about 20 Å of the SNAP/SNARE complex at the N end of the hexamer pore (Hohl et al., 1998). This association induces an ~15 Å dilation of the D1 ring diameter without any gross distortion of the D2 ring.

In order to gain insight into SNAP/SNARE complex binding and the mechanism of disassembly by NSF, we have determined the crystal structure of the N-terminal domain of NSF at 1.9 Å resolution. N contains two subdomains, a double ψ β barrel (Castillo et al., 1999), and a four strand–one helix α/β roll. The solvent-accessible surface features a large, very positively charged groove that could bind to the highly negative, α-helical, C-terminal region of α-SNAP (Rice and Brunger, 1999). Despite limited primary sequence similiarity, both subdomains are structurally similar to adjacent domains in EF-Tu, a protein that exhibits large nucleotide hydrolysis-dependent conformational changes (Jurnak and Abel, 1996). NSF and EF-Tu each contain a nucleotide-binding domain, D1 in NSF and domain 1 in EF-Tu, adjacent to these structurally similar subdomains. These similarities imply that both proteins may share a common hydrolysis-triggered conformational change. The insights obtained from this system will likely be generally applicable to other members of the AAA superfamily.

Results and Discussion

Structure Determination

Recombinant selenomethionine (Se–Met)-derivatized Chinese hamster ovary N was expressed in *E. coli*, purified to homogeneity, and crystallized by vapor diffusion. The crystal structure was solved to 1.9 Å resolution using multiwavelength anomalous diffraction (MAD) data collected at four wavelengths (Hendrickson, 1991) around the selenium absorption edge. The three ordered Se–Met sites were found by an automated Patterson search method (Grosse-Kunstleve and Brunger, 1999). After density modification with solvent flipping (Abrahams and Leslie, 1996) and histogram matching (Zhang and Main, 1990), an excellent, almost completely traceable, experimental electron density map was obtained (Figures 2A and 2B). The final model refined to an R_{free} value of 24.2% and includes residues 1–161 and 167–201, three sulfate ions, and 130 waters. Residues 162–166 and 202–205 were disordered.

The N-Terminal Domain Has Two Subdomains Sharing a Hydrophilic Interface

N contains two distinct subdomains (Figure 1A): N_A, residues 1–83, and N_B, residues 87–201. The predominantly

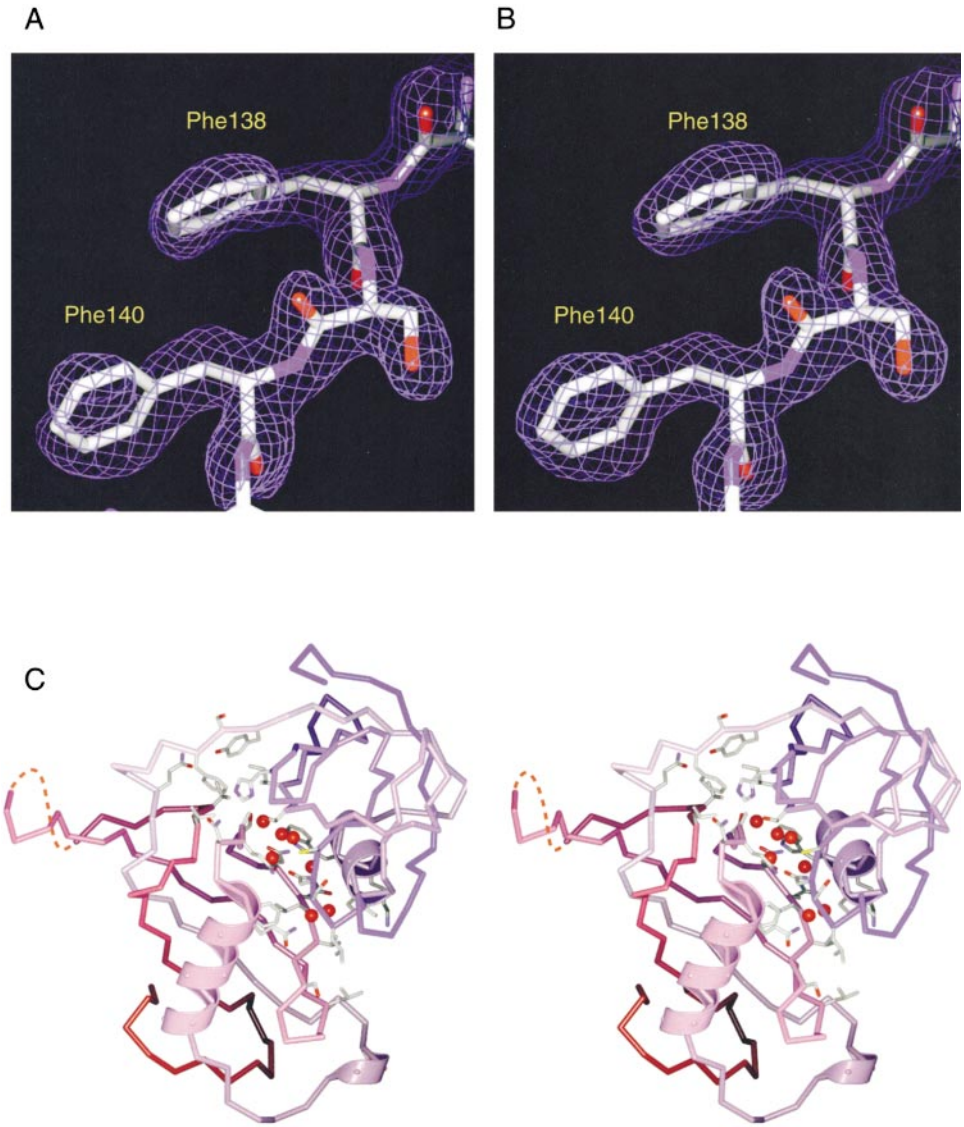

Figure 2. Representative Electron Density and Subdomain Interface

(A) Density-modified experimental map around Phe-138, contoured at 1.5 σ.

(B) $2F_o - F_c$ map of same region as (A), contoured at 1.5 σ and calculated with both model and experimental phases.

(C) Stereo rendition of buried water molecules (red spheres) in the interface region between subdomains N_A (blue) and N_B (red). Side chains of interface residues are drawn as gray sticks, and helices α1, α2′, and α3′ are rendered as ribbons. Red dashed line indicates disordered residues 162–166.

hydrophilic interface between the two subdomains buries approximately 1500 Å^2 and contains seven well-ordered water molecules (Figure 2C). The mean shape complementarity index (<Sc>) of the buried surfaces (Lawrence and Colman, 1993) is 0.567, well below 0.70, the average value expected for normal protein–protein interfaces; the values of <Sc> range from 0 to 1, for zero to perfect surface complementarity, respectively. Upon including the seven ordered water molecules, <Sc> increases to 0.68, indicating that the buried water molecules substantially compensate for the lack of shape complementarity between the two subdomains. Additionally, two small hydrophobic clusters are found at the edges of the interface, in the region between strand β6 and helix α1′, and the area formed by helices α1 and α2, and strand β4′ (Figure 2C). While the hydrated interface between the two NSF subdomains suggests that these surfaces could be solvent exposed at little energetic cost, there is evidence that suggests that the two subdomains are stably packed together and act as a unit. First, the thermal factors of residues are lowest in the core of N, including interface residues. This could be an artifact of crystal packing forces, though in an independently solved structure of NSF-N containing three molecules of N per asymmetric unit (May et al., 1999), a similar distribution of low B factors along interface residues is also seen in all molecules of N. Second, thermal denaturation of N in solution, monitored by circular dichroism at 218 nm, showed a single sigmoidal transition (data not shown). This is consistent with N

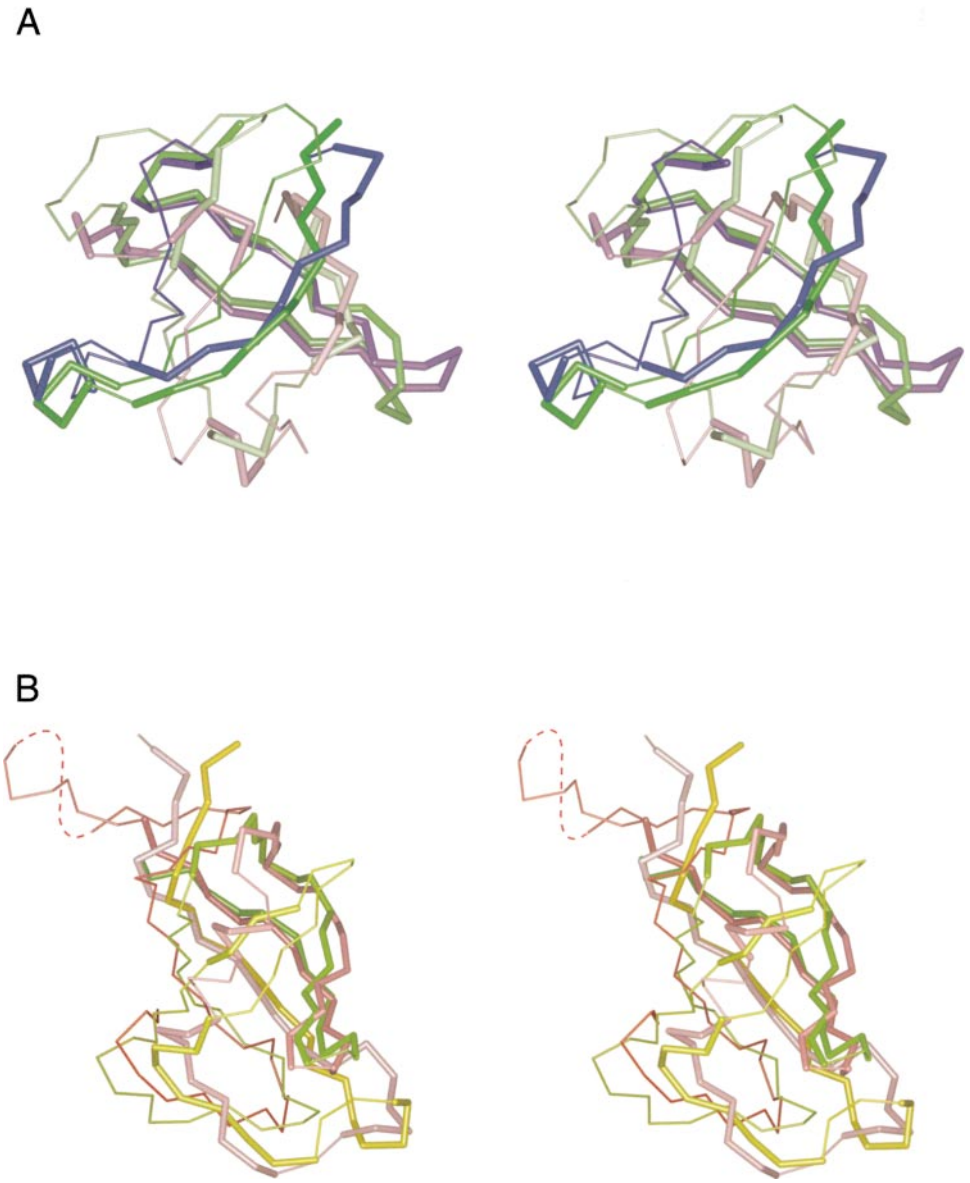

Figure 3. Structural Similarity between N and EF-Tu

Stereo backbone alignments of subdomains N_A and N_B to EF-Tu domains 2 and 3, respectively. Thick segments are considered equivalent by DALI and were used for C_α alignment. (A) N_A from blue (N terminus) to pink (C terminus), EF-Tu domain 2 from dark green to light green. (B) N_B from pink to red, EF-Tu from light green to yellow. Equivalent strands from N_A and EF-Tu domain 2 align with a C_α rmsd of 2.9 Å, and those from N_B and EF-Tu domain 3 align with a C_α rmsd of 3.2 Å. Red dashed line indicates disordered residues 162–166.

existing as a compact, single domain. A more complicated biphasic melting behavior would be expected if the structurally distinct N_A and N_B domains were separable in solution and denatured independently.

The N-Terminal Subdomain Is a Double-ψ β Barrel

Structural similarity searches using DALI (Holm and Sander, 1993) with N_A as a target yielded several proteins containing a recently described double-ψ β barrel (DPBB) motif (Castillo et al., 1999), such as DMSO reductase, aspartate decarboxylase, formate dehydrogenase, barwin, and fucose isomerase (Table 1). In fact, NSF homologs such as CDC-48p and the transitional endoplasmic reticulum ATPase (TERA) were predicted, on the basis of primary sequence analyses, to contain a DPBB motif. The aligned strands between N_A and the similar DPBB proteins overlap with C_α rmsd's ranging from 2.3 to 2.9 Å. The DPBB motif contains two interlocking ψ loops, which are strand–loop arrangements roughly resembling the Greek letter ψ (Figure 1C). The first ψ loop consists of strand β5 and the loop between strands β1 and β2; the second consists of strand β2 and the loop between strands β4 and β5. The topology of N_A is identical to that of the canonical DPBB except for a relocation of helix α1 from the consensus position between strands β2 and β3 to the first ψ loop region (Figure 1B). This disrupts the two-fold pseudosymmetry of the strand topology and places both helix α1 and α2

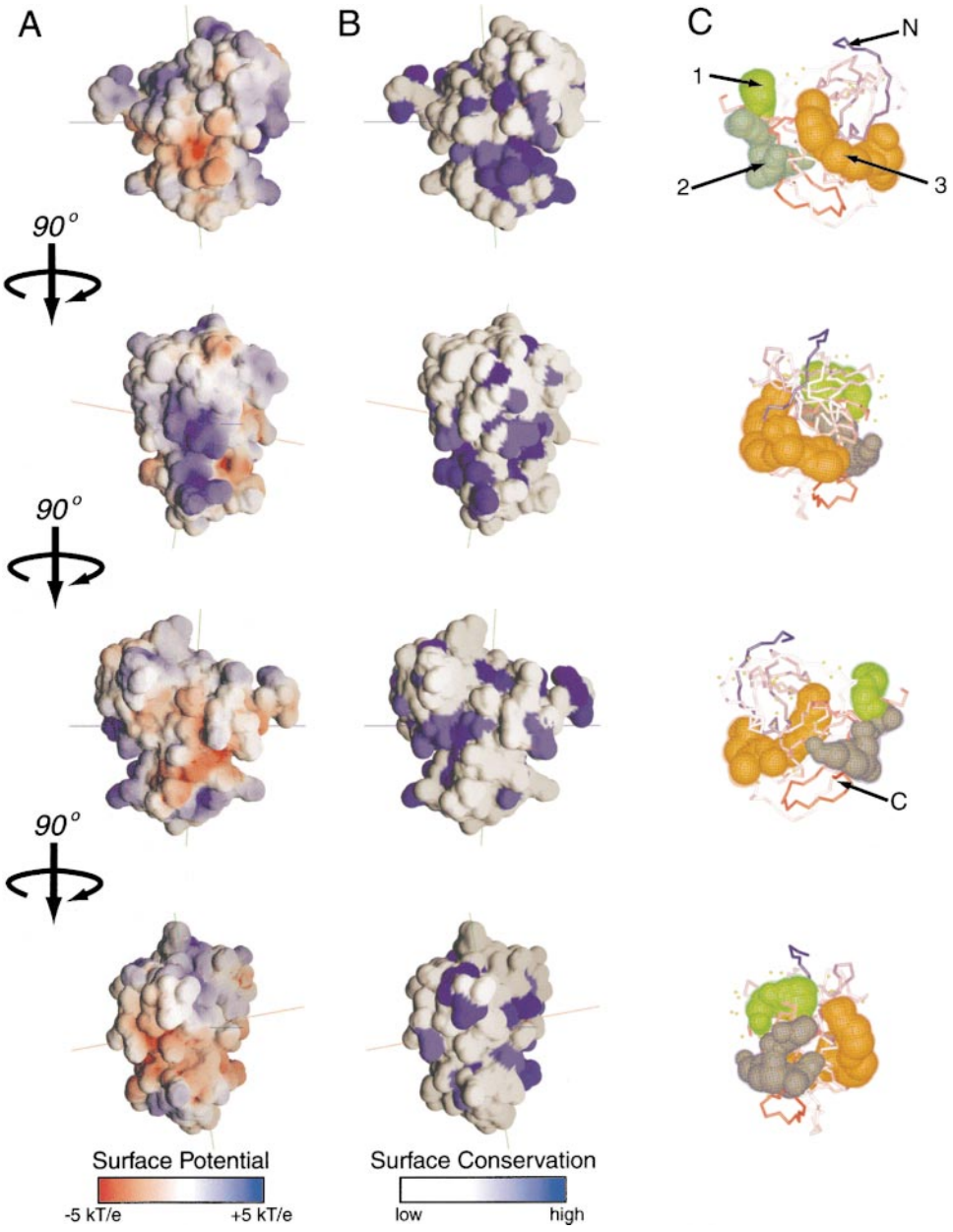

Figure 4. Surface Features of N

Right-handed 90° rotations from top to bottom row are shown.

(A) Surface of N colored according to the electrostatic potential computed by GRASP (Nicholls et al., 1991) using OPLS charges (Jorgensen and Tirado-Rives, 1988). The electrostatic surface was contoured between −5 kT/e (red) and +5 kT/e (blue).

(B) Primary sequence conservation of residues mapped to solvent-accessible surface.

(C) Cavities found using a 2.0–5.0 Å radius probe computed by SURFNET (Laskowski, 1995). Grooves are labeled 1 (light green), 2 (blue-green), and 3 (orange). Note that groove 3 overlaps with a very positive cavity in (A) and conserved regions in (B), making it a likely binding site for the negatively charged, helical C terminus of α-SNAP.

along one edge of a major surface groove in N. One common feature of DPBB motif–containing proteins is a catalytic or substrate-binding site in the ψ loop regions, found between strands β1 and β2, and between strands β3 and β4 (Castillo et al., 1999). This may indicate a substrate-binding region in N at this ψ loop.

Interestingly, domain 2 of EF-Tu is also structurally similar to N_A (Table 1; Figure 3B). Both are small six-stranded β barrels with shear numbers of 10, though EF-Tu domain 2 is topologically a Greek key β barrel rather than a DPBB. The core β strands of the barrels in the EF-Tu domain 2 and in N_B align with a C_α root-mean-square difference (rmsd) of 2.9 Å (Table 1).

The C-Terminal Subdomain Is an α/β Roll

N_B is a roll consisting of one α helix, α3′, and four β strands, β1′, β4′, β5′, and β7′ (Figure 1A). Helix α3′ is capped by two small two-stranded β sheets, antiparallel

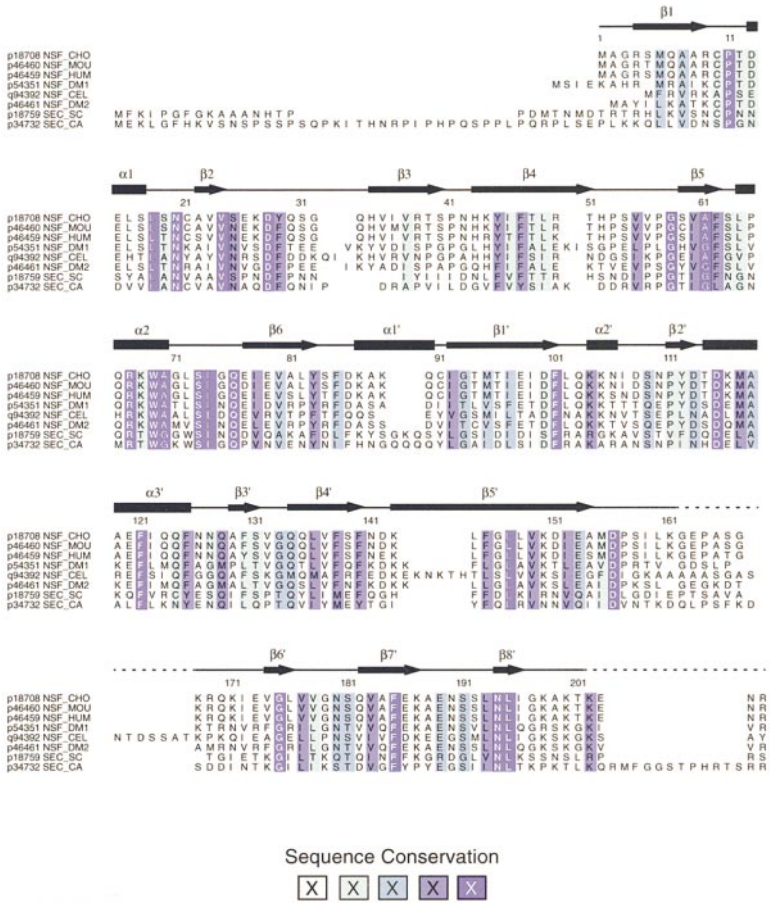

Figure 5. Sequence Alignment of CHO NSF to Other Known Orthologs

CHO NSF aligned with mouse, human, *Drosophila* (two isoforms), *C. elegans*, yeast *S. cerevisae*, and yeast *C. albicans*. Sequences were aligned using ClustalW (Thompson et al., 1994), then conservation values were calculated with AMAS (Livingstone and Barton, 1993). Colors indicated weak (light blue) to absolute (violet with white lettering) conservation. The top line indicates regions of β sheet strand (arrow) and α- or 3_{10}-helix (box) as assigned by DSSP (Kabsch and Sander, 1983). Numbers indicate residue number of CHO NSF. The dashed line indicates disordered regions.

strands β3′ and β6′, and parallel strands β2′ and β8′. The core of the roll between helix α3′ and strands β1′, β4′, and β5′ is made up of a peculiar row of highly conserved phenylalanine and tyrosine side chains (Figure 2), which form a ladder of aromatic side chains (Figure 1D).

Surprisingly, another domain of EF-Tu, domain 3, was the sole structure in the representative structure database identified by DALI as being similar to N_B (Table 1). The topologies between N_B and domain 3 of EF-Tu, a six-stranded jelly roll β barrel, are not identical, but four β strands, consisting of 61 residues, closely superimpose with a C_α rms deviation of 3.2 Å (Figure 3; Table 1).

Surface Charge, Conservation, and Shape

The 10,500 Å^2 solvent-accessible surface is highly textured, with many knobs and grooves. It possesses an overall positive charge (Figure 4A) and, compared to known orthologs (Figure 5), shows concentrated patches of primary sequence conservation (Figure 4B). Positive charges are primarily localized to two areas: near the disordered loop in N_B between strands β5′ and β6′, and in the large groove formed by helices α1 and α2, and strand β4′ (Figure 4A). Negative charges are found on faces of the protein away from the large positive groove. Primary sequence conservation of the accessible surface clusters into two regions: a small patch near the disordered loop, and a much larger streak along the intersubdomain cavity, starting at the lower half of the groove along N_B and terminating on the other side of the protein along the surface of N_A.

A cavity analysis performed by SURFNET (Laskowski, 1995) using a 2.0–5.0 Å radius probe identified three grooves, all large enough to potentially accommodate a typical α helix (Figure 4C). Grooves 1 and 2 are above

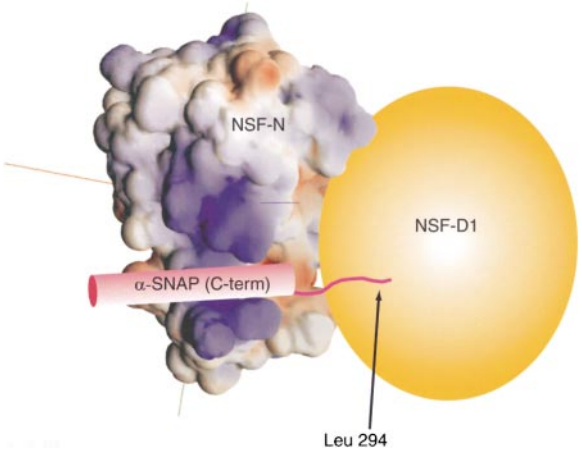

Figure 6. Model of α-SNAP Binding to Groove 3 of N

Assuming that the position of D1 is near the C terminus of N, binding of the C terminus of α-SNAP to groove 3 would allow for the penultimate residue of α-SNAP to interact with D1.

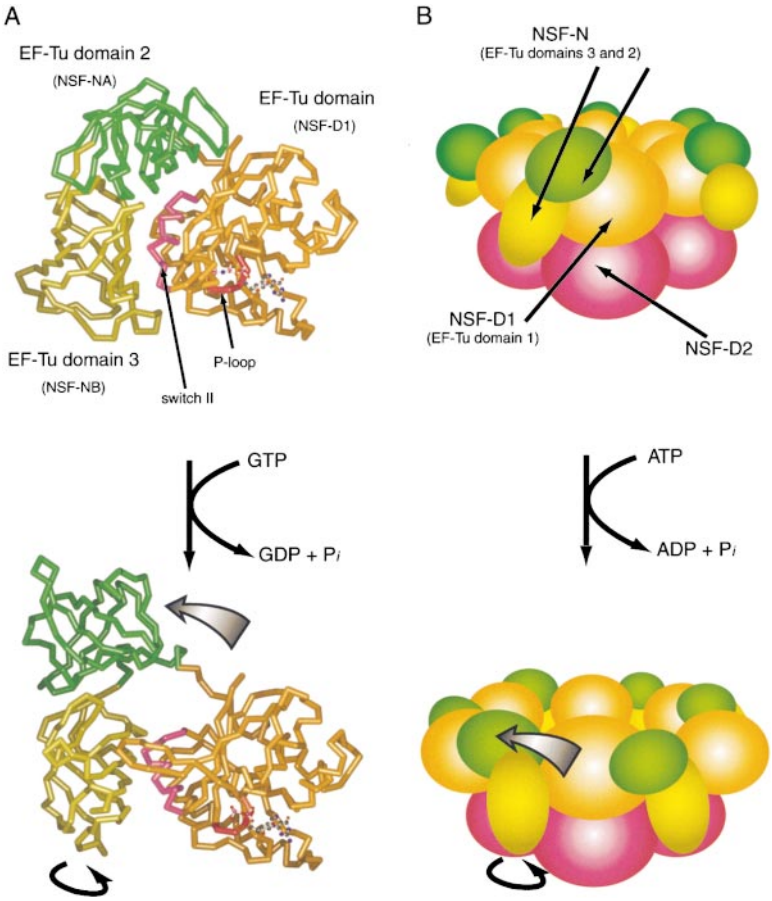

Figure 7. Model of Conformational Changes in NSF Based on the Structural Similarity to EF-Tu

(A) Nucleotide-dependent conformation of EF-Tu. The switch II helix, which changes conformation upon loss of the gamma phosphate of the bound nucleotide, is shown in purple. The nucleotide, drawn in ball-and-stick, is cradled by the conserved P loop region, drawn in red. The GMPPNP- (top) and GDP-bound (bottom) conformations are aligned by a least-squares fit of the P loop and nucleotide atoms in domain 1 (orange). Upon nucleotide hydrolysis, domains 2 (green) and 3 (yellow) twist and move back into the plane of the figure and remain fixed relative to each other during this rotation. During this movement, domain 1 swings approximately 90° about an axis through domains 2 and 3. PDB accession codes for GMPPNP- and GDP-bound EF-Tu are 1EFT (Kjeldgaard et al., 1993) and 1TUI (Polekhina et al., 1996), respectively.

(B) Model of nucleotide-dependent motions in an NSF hexamer, held together by a ring of D2 domains (red). In the ATP-charged state, the N domains (yellow and green) are flared outward from the pore of the hexamer. After ATP hydrolysis, N rotates and twists relative to D1 (orange). This model is consistent with estimated hexamer dimensions derived from EM studies (Hanson et al., 1997; Hohl et al., 1998).

and below the disordered loop, respectively. Groove 3 closely follows the pattern of conserved exposed surface area described above. It starts near the top of the aromatic residue ladder region of N_B, follows the α helix, then turns to cross the junction between subdomains, into a slightly negatively charged concave region defined by helix α2 and strands β1′, β4′, and β5′.

The Putative α-SNAP Binding Site

The crystal structure of N and the recently solved structure of the yeast SNAP Sec17 (Rice and Brunger, 1999) suggest possible modes of interactions between NSF and α-SNAP. Assuming structural similarity between Sec17 and α-SNAP, the C-terminal portion of α-SNAP, necessary for NSF binding and ATPase stimulation (Barnard et al., 1996, 1997), is predominantly α-helical and negatively charged. Surface charge, sequence conservation, and shape limit potential α-SNAP-binding sites on N to two of the three surface cavities (Figure 4C). While all three are large enough to bind an α helix, the predominantly negative charge of groove 2 (Figure 4A) makes it an unlikely binding site. Though groove 1 is weakly positively charged and conserved, groove 3 is more likely to interact with α-SNAP since it has the highest local concentration of positive charge and sequence conservation (Figure 4C). Interestingly, groove 3 contains the first N_A ψ loop, which serves as a binding or catalysis site in many DPBB proteins (Castillo et al., 1998).

Leucine 294 of α-SNAP, a residue implicated in D1 nucleotide hydrolysis stimulation (Barnard et al., 1997), is C-terminal to the ultimate α helix, just outside the region of ordered electron density in the crystal structure of Sec17 (Rice and Brunger, 1999). The hydrolysis-stimulating effect of this residue suggests a direct interaction with D1. If one assumes that the C terminus of N points to the general location of D1, groove 3 could bind the C-terminal α helix of α-SNAP such that Leu-294 would be in the vicinity of D1 (Figure 6). At present, the orientation of D1 relative to N and the extent to which α-SNAP contacts D1 are unknown. In fact, the isolated N domain does not bind to the SNAP/SNARE complex, while constructs of N with an adjacent ATPase domain (N-D1 and N-D2) do (Nagiec et al., 1995). One explanation for this characteristic is that the presence of the D1 domain induces a structural change in N necessary for proper α-SNAP binding. Another possibility is that the neighboring D1 or D2 also participates in binding to α-SNAP. For example, the N-terminal portion of the ATP-binding domain of AAA yeast protease Yme1p, which is similar to D1, is able to specifically bind substrate (Leonhard et al., 1999). Currently it is difficult to distinguish between these and other possibilities.

A Model of NSF Domain Motion

The conformational changes observed by EM in NSF upon ATP hydrolysis may provide a mechanical force used to disassemble the SNARE complex. In light of the

Table 2. Crystallographic Data and Phasing[a]

Crystal Information						
Crystal	Space Group		Cell Dimensions			
Se–Met	$C222_1$		a = 32.04 Å, b = 175.36 Å, c = 79.66 Å, $\alpha = \beta = \gamma = 90°$			
Data Statistics						
Crystal	d_{min} Å	Total Number of Reflections	Average Redundancy	Completeness (%)	I/σ	R_{sym}[b] (%)
Se–Met λ_1 (0.9799 Å)	1.9	32,855	3.6 (2.6)	97.8 (89.8)	21.3 (6.6)	6.0 (20.3)
Se–Met λ_2 (0.9801 Å)	1.9	33,269	3.9 (2.6)	98.4 (90.5)	22.8 (5.9)	5.8 (24.8)
Se–Met λ_3 (0.9998 Å)	1.9	33,216	3.2 (2.7)	98.0 (92.7)	20.4 (5.1)	5.7 (27.0)
Se–Met λ_4 (0.9537 Å)	1.9	33,652	3.6 (3.1)	98.7 (97.9)	18.8 (2.8)	7.4 (58.4)

Observed Diffraction Ratios[c]				
	λ_1	λ_2	λ_3	λ_4
λ_1	0.062	0.060	0.090	0.110
λ_2		0.045	0.062	0.085
λ_3			0.053	0.070
λ_4				0.078

Two-Wavelength MAD Phasing Power[d], 16.66–1.90 (1.98–1.90) Å		
$\lambda_2 \rightarrow \lambda_2^-$	$\lambda_2 \rightarrow \lambda_1^+$	$\lambda_2 \rightarrow \lambda_1^-$
0.74 (0.17)	0.69 (0.29)	1.11 (0.33)

SAD Phasing Power[d], 16.66–1.90 (1.99–1.90) Å		
$\lambda_1 \rightarrow \lambda_1^-$	$\lambda_2 \rightarrow \lambda_2^-$	$\lambda_3 \rightarrow \lambda_3^-$
1.00 (0.13)	0.39 (0.00)	0.35 (0.00)

Figures of Merit (FOM)	
	FOM
Two-wavelength ($\lambda 1 \lambda 2$) MAD	0.36 (0.15)
λ_1 SAD	0.17 (0.03)
λ_2 SAD	0.04 (0.00)
λ_3 SAD	0.05 (0.00)
Combined FOM[e]	0.39 (0.13)

[a] Values in parentheses are for the high-resolution bin, 1.97–1.90 Å.
[b] $R_{sym} = \Sigma_h \Sigma_i |I_i(h) - \langle I(h) \rangle| / \Sigma_h \Sigma_i I_i(h)$, where $I_i(h)$ is the i^{th} measurement and $\langle I(h) \rangle$ is the mean of all measurements of I(h) for Miller indices h.
[c] Values are $\langle(\Delta|F|)^2\rangle^{1/2} / \langle|F|^2\rangle^{1/2}$, where $\Delta|F|$ is the dispersive (off-diagonal elements), or Bijvoet difference (diagonal elements), computed between 20 and 2.6 Å resolution.
[d] MAD phasing power is defined as $[\langle|F_D - F_N^2\rangle / \int_\phi P(\phi)(||F_N| e^{i\phi} + \Delta F_h| - |F_D|)^2 d\phi]^{1/2}$, where $P(\phi)$ is the experimental phase probability distribution. F_N corresponds to the structure factors at the reference wavelength λ_2, F_D corresponds to the structure factors at wavelength λ_i (indicated by a superscript plus) or its Friedel mate (indicated by a superscript minus), and ΔF_h is the difference in heavy atom structure factors between the two wavelengths. SAD phasing power is the same except the reference wavelength is λ_i.
[e] Figure of merit of phase probability distribution combined from one two-wavelength MAD phase distribution and three one-wavelength SAD phase distributions.

structural similarities between the N- and C-terminal subdomains in N and domains 2 and 3 of EF-Tu, respectively, we propose that NSF generates similar large domain motions between N and D1 upon nucleotide hydrolysis. It should be noted that the connectivities of the analogous domains are different: the nucleotide-binding domain of EF-Tu is N-terminal to domains 2 and 3, while it is C-terminal to N_A and N_B in NSF. However, these topological differences do not necessarily rule out the possibility of similar domain motions. Comparing the GMPPNP- and GDP-bound crystal structures of EF-Tu (Figure 7A), the loss of the nucleotide γ phosphate induces a structural change in the α helix that forms the switch II region, disrupting contacts between the nucleotide-binding domain and domains 2 and 3 of EF-Tu (Kjeldgaard et al., 1993). This structural change triggers a large movement of EF-Tu domain 1, a rotation of over 90° about an axis through EF-Tu domains 2 and 3 (Figure 7A). EF-Tu domains 2 and 3 essentially move together as a rigid unit during this rotation. One could imagine a similar large relative domain movement between N and D1 (Figure 7B), assuming that both domains are stable, folded structures. The proposed motion in each NSF protomer upon ATP hydrolysis, if transmitted through α-SNAPs, could lead to an unwinding or opening of the bound SNARE complex. Clearly, this model is speculative since the position of D1 relative to N is unknown. However, the model is consistent with the conformational changes observed in EM studies (Hanson et al., 1997).

Experimental Procedures

Cloning and Expression

DNA encoding Chinese hamster ovarian N was subcloned from full-length NSF using PCR with the following primers, 5′–3′: GGAATTCA

Table 3. Refinement Statistics

Resolution (Å)	Overall (50.0–1.9)	50.0–4.09	3.25	2.84	2.58	2.39	2.25	2.14	2.05	1.97	1.90
R value[a]	21.0	22.5	19.4	20.4	21.8	21.3	20.5	19.9	20.0	21.3	24.0
R_{free} value[b]	24.2	24.0	21.8	26.8	24.2	25.9	24.0	24.5	23.2	24.5	28.1
Luzzati coordinate error	0.22 Å										
Cross-validated Luzzati coordinate error	0.26 Å										
Bond length deviation	0.010 Å										
Bond angle deviation	1.42°										
Improper angle deviation	0.79°										
Dihedrals	25.34°										
Average B factor	25.53 $Å^2$										
Minimum B factor	10.72 $Å^2$										
Maximum B factor	70.06 $Å^2$										
Residues in core regions (%)	95.0%										
Residues in disallowed regions (%)	0.0%										
Number of reflections	32,739										

[a] $R = \Sigma(|F_{obs}| - k|F_{calc}|)/\Sigma|F_{obs}|$.
[b] R_{free} value is the R value obtained for a test set of reflections, consisting of a randomly selected 10% subset of the diffraction data, not used during refinement.

TTAATATGGCGGGCCGGAGTATGCAAGC and GAATTCCTGATCA CTCGAGGCGATTTTCCTTGGTTTTAGC. N was subcloned into the pET15b expression vector (Novagen). The resulting protein contained a thrombin-cleavable N-terminal hexahistidine tag. All DNA sequences were verified by dideoxynucleotide sequencing (HHMI Biopolymer and W. M Keck, Biotechnology Resource Laboratory, Yale University). The expression construct was transformed into BL21λ(DE3) cells (Novagen). Cells were grown in M9 minimal medium containing 150 mg/l ampicillin at 37°C. At an optical density of $A_{600nm} = 2.0$, methionine synthesis was inhibited by adding 100 mg/l D-lysine, D-phenylalanine, and D-threonine; 50 mg/l D-isoleucine and D-valine; and 60 mg/l D/L selenomethionine (Sigma). After 15 min, cells were induced with 0.4 mM isopropyl-1-β-D-thiogalactopyranoside. Four hours later, cells were harvested by centrifugation and stored at −80°C. Frozen cells (20 g) were thawed and homogenized in 100 ml of buffer A (20 mM HEPES [pH 7.8], 500 mM NaCl, 10 mM 2-mercaptoethanol) and 0.1% Triton X-100, then lysed by sonication. The lysate was centrifuged for 30 min at 40,000 × g. The supernatant was loaded by gravity over a column packed with 10 ml of Ni-NTA resin (Qiagen). A 100 ml linear gradient was run from 100% buffer A to 100% buffer A + 300 mM imidazole (pH 8.0). The hexahistidine-tagged protein eluted at approximately 100 mM imidazole. Fractions containing N (as judged by Coomassie blue–stained SDS-PAGE) were pooled, and the protein concentration was adjusted to 2 mg/ml. Thrombin (Haematologic Technologies, Inc.) was added at 0.5 mg l^{-1}, and the mixture was dialyzed for 12 hr against buffer C (20 mM HEPES [pH 7.2] 10 mM dithiothreitol [DTT]) + 50 mM NaCl. After dialyzing, the protein was loaded onto a Mono S column (Pharmacia) and eluted with a 10 column volume linear gradient from 100% buffer C to 100% buffer C + 500 mM NaCl. N eluted at approximately 150 mM NaCl. Fractions containing N were concentrated to 10 mg/ml and dialyzed against buffer C + 150 mM NaCl for 12 hr. Protein concentrations were determined using the Bradford protein concentration assay (Bio-Rad) calibrated with a bovine serum albumin standard.

Crystallization, Data Collection, and Processing

Initial crystals grew by hanging drop vapor diffusion at 20°C. Two microliters of 10 mg/ml protein was mixed with 2 μl of mother liquor, consisting of 100 mM Tris (pH 8.7), 2.0 M ammonium sulfate, and 10 mM DTT, on a siliconized glass cover slip and equilibrated against 0.5 ml of mother liquor. Rod-shaped crystals grew to full size (100 μm × 20 μm × 20 μm) after 48 hr. Several crystals were crushed and resuspended in 0.2 ml of mother liquor for use as a seed stock for later streak seeding. Larger crystals were grown by sitting drop vapor diffusion at 20°C. Five microliters of 10 mg/ml protein was mixed with 5 ml of mother liquor and equilibrated for 12 hr. The drops were then streak seeded using the seed stock. Crystals grew to full size (200 μm × 40 μm × 40 μm) in 48 hr. Crystals were cryoprotected by sequential transfer into mother liquor with 5%–30% glycerol, and then flash frozen in liquid nitrogen–cooled propane.

N crystallized in space group $C222_1$ with one molecule per asymmetric unit. The solvent content of the crystal was approximately 52%. MAD data were collected using four wavelengths (Table 2) at 100 K at beamline 5.0.2 at the Advanced Light Source (Berkeley, CA) using a Quantum-4 CCD detector (Area Detector Systems Corporation). Inverse beam geometry was employed using 15° wedges. The diffraction data was collected one wavelength at a time. Data were processed using DENZO (Otwinowski and Minor, 1997), and intensities were reduced and scaled using SCALEPACK (Otwinowski and Minor, 1997) (Table 1).

Structure Determination

Three of the five expected selenium sites of N were found in anomalous difference Patterson maps calculated at the peak anomalous (λ_1) wavelength using an automated Patterson heavy atom search method (Grosse-Kunstleve and Brunger, 1999). The two remaining sites, one at the N terminus and one in a disordered loop, were disordered and could not be placed. The MAD data suffered from problems associated with the dispersive signals (Table 1), which increased as data collection progressed from λ_1 to λ_4. This is apparent in the observed diffraction ratios, where the largest dispersive difference occurred between the two remote wavelengths. Normally, this dispersive difference is expected to be rather small. This systematic error was presumably introduced by collecting the MAD data one wavelength at a time, exacerbating the effects of radiation damage that are present even at 100 K. It prevented the use of most dispersive differences for MAD phasing except for the dispersive differences between the peak (λ_1) and inflection (λ_2) wavelengths. Two-wavelength MAD phasing with diffraction data from peak (λ_1) and inflection point (λ_2) wavelengths used the Phillips-Hodgson (Phillips and Hodgson, 1980) method and site refinement against a maximum likelihood target (Burling et al., 1996) with λ_2 as the reference wavelength at 50–1.9 Å resolution. All anomalous differences were well behaved (Table 1). Thus, wavelengths with significant anomalous signal (λ_1, λ_2, and λ_4) were each used for single-wavelength anomalous diffraction (SAD) phasing and site refinement against a maximum likelihood target (Burling et al., 1996). Overall f′ and f′′ form factors of the Se–Met sites at a particular wavelength were refined against the MAD or SAD data. Phase probability distributions from the two-wavelength MAD and the three SAD refinements were multiplied with equal weighting. Density modification of these combined phase probability distributions was carried out using solvent flipping (Abrahams and Leslie, 1996) and histogram

matching (Zhang and Main, 1990). Density modification proved essential for producing traceable electron density maps. This procedure dramatically improved map quality and compensated significantly for the lack of dispersive information. All heavy atom search, phasing, and density modification calculations were carried out with the crystallography and NMR System (CNS) (Brunger et al., 1998).

Model Building and Refinement

The initial model was built using the program O (Jones et al., 1991). The high quality of the initial experimental electron density map and known selenium sites allowed unambiguous tracing for most of the protein backbone and side chain atoms. Progress was monitored with the R_{free} value using a 10% randomly selected test set. This test set was also used for cross-validation of σ_A and other statistical quantities required for the calculation of the maximum likelihood target and σ_A-weighted electron density maps. Initial refinement consisted of one iteration of torsion angle dynamics simulated annealing (Rice and Brunger, 1994) using the MLHL target function (Pannu and Read, 1998) with the experimental, density-modified phases as a prior phase distribution, followed by model rebuilding in O. Later, refinement consisted of iterative rounds of model building (including selecting chemically reasonable water molecules and sulfate ions) in phase-combined σ_A-weighted $2F_o - F_c$ maps (Read, 1986), conjugate gradient minimization, and individual restrained atomic B factor refinement (Hendrickson, 1985). Refinement was carried out against low energy remote (wavelength λ_3) diffraction data. Refinement used a flat bulk solvent correction (electron density level $\rho_{sol} = 0.40$ e/Å^3, $B_{sol} = 46.3$ Å^2 [Jiang and Brunger, 1994]) and overall anisotropic B factor correction ($B_{11} = 5.54$ Å^2, $B_{22} = 3.62$ Å^2, $B_{33} = -9.16$ Å^2, $B_{12} = 0.00$ Å^2, $B_{13} = 0.00$ Å^2, $B_{33} = 0.00$ Å^2) at 50–1.9 Å resolution. Final model statistics are shown in Table 3. The final model contains 130 water molecules and three sulfate ions. All refinement calculations were carried out with CNS (Brunger et al., 1998).

Figure Preparation

All figures were prepared using GL_Render (courtesy of Dr. L. Esser), Bobscript (Esnouf, 1997), Molscript (Kraulis, 1991), and Pov-Ray (The POV-ray Team, 1998) unless otherwise noted.

Acknowledgments

We thank R. B. Sutton for expert advice; L. Rice, C. Stroupe, M. Bowen, M. Wilson, J. Ernst, M. Reese, and J. Hyman for stimulating discussions and critical reading of the manuscript; and T. Earnest, L.-W. Hung, C. Stroupe, and L. Rice for help with data collection at beamline 5.0.2 at the Advanced Light Source (ALS is funded by the US Department of Energy Office of Basic Energy Sciences); and P. Adams and R. Grosse-Kunstleve for expert help with CNS.

Received April 29, 1999; revised June 7, 1999.

References

Abrahams, J.P., and Leslie, A.G.W. (1996). Methods used in the structure determination of bovine mitochondrial F1 ATPase. Acta Crystallogr. D *52*, 30–42.

Barnard, R.J.O., Morgan, A., and Burgoyne, R.D. (1996). Domains of α-SNAP required for the stimulation of exocytosis and for N-ethylmaleimide-sensitive fusion protein (NSF) binding and activation. Mol. Biol. Cell *7*, 693–701.

Barnard, R.J.O., Morgan, A., and Burgoyne, R.D. (1997). Stimulation of NSF ATPase activity by alpha-SNAP is required for SNARE complex disassembly and exocytosis. J. Cell Biol. *139*, 875–883.

Bennett, M.K., and Scheller, R.H. (1993). The molecular machinery for secretion is conserved from yeast to neurons. Proc. Natl. Acad. Sci USA *90*, 2559–2563.

Beyer, A. (1997). Sequence analysis of the AAA protein family. Prot. Sci. *6*, 2043–2058.

Brunger, A.T., Adams, P.D., Clore, G.M., Gros, P., Grosse-Kunstleve, R.W., Jiang, J.-S., Kuszewski, J., Nilges, M., Pannu, N.S., Read, R.J., et al. (1998). Crystallography and NMR system (CNS): a new software system for macromolecular structure determination. Acta Crystallogr. D *54*, 905–921.

Burling, F.T., Weis, W.I., Flaherty, K.M., and Brunger, A.T. (1996). Direct observation of protein solvation and discrete disorder with experimental crystallographic phases. Science *271*, 72–77.

Castillo, R.M., Mizuguchi, K., Dhanaraj, V., Albert, A., Blundell, T.L., and Murzin, A.G. (1999). A six-stranded double-psi beta barrel is shared by several protein superfamilies. Structure *7*, 227–236.

Confalonieri, F., and Duguet, M. (1995). A 200 amino acid ATPase module in search of a basic function. Bioessays *17*, 639–650.

Esnouf, R.M. (1997). Bobscript: an extensively modified version of MolScript that includes greatly enhanced coloring capabilities. J. Mol. Graph. Model *15*, 132–134.

Ferro-Novick, S., and Jahn, R. (1994). Vesicle fusion from yeast to man. Nature *370*, 191–193.

Fleming, K.G., Hohl, T.M., Yu, R.C., Muller, S.A., Wolpensinger, B., Engel, A., Engelhardt, H., Brünger, A.T., Söllner, T.H., and Hanson, P.I. (1998). A revised model for the oligomeric state of the N-ethylmaleimide-sensitive fusion protein, NSF. J. Biol. Chem. *273*, 15675–15681.

Grosse-Kunstleve, R.W., and Brunger, A.T. (1999). A highly automated heavy-atom search procedure for macromolecular structures. Acta Crystallogr. D, in press.

Hanson, P.I., Roth, R., Morisaki, H., Jahn, R., and Heuser, J.E. (1997). Structure and conformational changes in NSF and its membrane receptor complexes visualized by quick-freeze/deep-etch electron microscopy. Cell *90*, 523–535.

Hay, J.C., and Scheller, R.H. (1997). SNAREs and NSF in targeted membrane fusion. Curr. Opin. Cell Biol. *9*, 505–512.

Hayashi, T., McMahon, H., Yamasaki, S., Binz, T., Hata, Y., Südhof, T.C., and Niemann, H. (1994). Synaptic vesicle membrane fusion complex: action of clostridial neurotoxins on assembly. EMBO J. *13*, 5051–5061.

Hayashi, T., Yamasaki, S., Nauenburg, S., Binz, T., and Niemann, H. (1995). Disassembly of the reconstituted synaptic vesicle membrane fusion complex in vitro. EMBO J. *14*, 2317–2325.

Hendrickson, W.A. (1985). Stereochemically restrained refinement of macromolecular structures. Methods Enzymol. *115*, 252–270.

Hendrickson, W.A. (1991). Determination of macromolecular structures from anomalous diffraction of synchotron radiation. Science *254*, 51–58.

Hohl, T.M., Paralti, F., Wimmer, C., Rothman, J.E., Söllner, T.H., and Engelhardt, H. (1998). Arrangement of subunits in 20S particles consisting of NSF, SNAPs, and SNARE complexes. Mol. Cell *2*, 539–548.

Holm, L., and Sander, C. (1993). Protein structure comparison by alignment of distance matrices (Dali 2.0). J. Mol. Biol. *233*, 123–138.

Jiang, J.S., and Brunger, A.T. (1994). Protein hydration observed by x-ray diffraction: solvation properties of penicillopepsin and neuraminidase crystal structures. J. Mol. Biol. *243*, 100–115.

Jones, T.A., Zou, J.Y., Cowan, S., and Kjeldgaard, M. (1991). Improved methods for building protein models in electron density maps and the location of errors in these models. Acta Crystallogr. A *47*, 110–119.

Jorgensen, W.L., and Tirado-Rives, J. (1988). The OPLS potential functions for protein energy minimizations for crystals of cyclic peptide and crambin. J. Am. Chem. Soc. *110*, 1657–1666.

Jurnak, F., and Abel, K. (1996). A complex profile of protein elongation: translating chemical energy into molecular movement. Structure *4*, 229–238.

Kabsch, W., and Sander, C. (1983). Dictionary of protein secondary structure: pattern recognition of hydrogen-bonded and geometrical features. Biopolymers *22*, 2577–2637.

Kjeldgaard, M., Nissen, P., Thirup, S., and Nyborg, J. (1993). The crystal structure of elongation factor EF-Tu from *Thermus aquaticus* in the GTP conformation. Structure *1*, 35–50.

Kraulis, P. (1991). MOLSCRIPT: a program to produce both detailed and schematic plots of protein structures. J. Appl. Crystallogr. *24*, 946–950.

Laskowski, R.A. (1995). SURFNET: a program for visualizing molecular surfaces, cavities and intermolecular interactions. J. Mol. Graph. *13*, 323–330.

Lawrence, M.C., and Colman, P.M. (1993). Shape complementarity at protein/protein interfaces. J. Mol. Biol. *234*, 946–950.

Leonhard, K., Stiegler, A., Neupert, W., and Langer, T. (1999). Chaperone-like activity of the AAA domain of the yeast Yme1 AAA protease. Nature *398*, 348–350.

Lenzen, C.U., Steinmann, D., Whiteheart, S.W., and Weis, W.I. (1998). Crystal structure of the hexamerization domain of N-ethylmaleimide-sensitive fusion protein. Cell *94*, 525–536.

Livingstone, C.D., and Barton, G.J. (1993). Protein sequence alignments: a strategy for the hierarchical analysis of residue conservation. Comput. Appl. Biosci. *9*, 745–756.

May, A.P., Misura, K.M.S., Whiteheart, S.W., and Weis, W.I. (1999). Crystal structure of the amino-terminal domain of *N*-ethylmaleimide-sensitive fusion protein. Nat. Cell Biol. *1*, 175–182.

Morgan, A., and Burgoyne, R.D. (1995). A role for the soluble NSF attachment proteins (SNAPs) in regulated exocytosis in adrenal chromaffin cells. Eur. Mol. Biol. Organ. J. *14*, 232–239.

Morgan, A., Dimaline, R., and Burgoyne, R.D. (1994). The ATPase activity of N-ethylmaleimide-sensitive fusion protein NSF is regulated by soluble NSF attachment proteins. J. Biol. Chem. *269*, 29347–29350.

Nagiec, E.E., Bernstein, A., and Whiteheart, S.W. (1995). Each domain of N-ethylmaleimide-sensitive fusion protein contributes to its transport activity. J. Biol. Chem. *49*, 29182–29188.

Nicholls, A., Sharp, K.A., and Honig, B. (1991). Protein folding and association: insights from the interfacial and thermodynamic properties of hydrocarbons. Proteins *11*, 281–296.

Otwinowski, Z., and Minor, W. (1997). Processing of x-ray diffraction data collected in oscillation mode. Methods Enzymol. *276*, 307–326.

Pannu, N.S., and Read, R.J. (1996). Improved structure refinement through maximum likelihood. Acta Crystallogr. A *52*, 659–668.

Patel, S., and Latterich, M. (1993). The AAA team: related ATPases with diverse functions. Trends Cell Biol. *8*, 65–71.

Phillips, J.C., and Hodgson, K.O. (1980). The use of anomalous scattering effects to phase diffraction patterson from macromolecules. Acta Crystallogr. A *36*, 856–864.

Polekhina, G., Thirup, S., Kjeldgaard, M., Nissen, P., Lippmann, C., and Nyborg, J. (1996). Helix unwinding in the effector region of elongation factor EF-Tu-GDP. Structure *4*, 1141–1151.

The POV-ray Team. (1998). Pov-ray—the persistence of vision raytracer (http://www.povray.org/) (Indianapolis, IN: Cyborg Software Systems, Inc.).

Read, R.J. (1986). Improved Fourier coefficients for maps using phases from partial structures with errors. Acta Crystallogr. A *42*, 140–149.

Rice, L.M., and Brunger, A.T. (1994). Torsion angle dynamics: reduced variable conformational sampling enhances crystallographic structure refinement. Proteins *19*, 277–290.

Rice, L.M., and Brunger, A.T. (1999). Crystal structure of the vesicular transport protein Sec17: implications for SNAP function in SNARE complex disassembly. Mol. Cell *4*, this issue, 85–95.

Rothman, J.E. (1996). The protein machinery of vesicle budding and fusion. Prot. Sci. *5*, 185–194.

Söllner, T., Bennett, M.K., Whiteheart, S.W., Scheller, R.H., and Rothman, J.E. (1993). A protein assembly-disassembly pathway in vitro that may correspond to sequential steps of synaptic vesicle docking, activation, and fusion. Cell *75*, 409–418.

Sumida, M., Hong, R.-M., and Tayaga, M. (1994). Role of two nucleotide-binding regions in an N-ethylmaleimide-sensitive factor involved in vesicle-mediated protein transport. J. Biol. Chem. *269*, 20636–20641.

Sutton, R.B., Fasshauer, D., Jahn, R., and Brunger, A.T. (1998). Crystal structure of a SNARE complex involved in synaptic exocytosis at 2.4 Å resolution. Nature *395*, 347–353.

Tayaga, M., Wilson, D.W., Brunner, M., Arango, N., and Rothman, J.E. (1993). Domain structure of an N-ethylmaleimide-sensitive fusion protein involved in vesicular transport. J. Biol. Chem. *268*, 2662–2666.

Thompson, J.D., Higgins, D.G., and Gibson, T.J. (1994). CLUSTAL W: improving the sensitivity of progressive multiple sequence alignment through sequence weighting, positions specific gap penalties and weight matrix choice. Nucleic Acids Res. *22*, 4673–4680.

Walker, J.E., Saraste, M.J., Runswick, J.J., and Gay, N.J. (1982). Distantly related sequences in the beta- and gamma-subunits of ATPase, myosin, kinases and other ATP-requiring enzymes and a common nucleotide binding fold. EMBO J. *1*, 945–951.

Weber, T., Zemelman, B.V., McNew, J.A., Westermann, B., Gmachl, M., Parlati, F., Söllner, T.H., and Rothman, J.E. (1998). SNAREpins: minimal machinery for membrane fusion. Cell *92*, 759–772.

Wilson, D.W., Whiteheart, S.W., Wiedmann, M., Brunner, M., and Rothman, J.E. (1992). A multisubunit particle implicated in membrane fusion. J. Cell Biol. *117*, 531–538.

Whiteheart, S.W., Brunner, M., Wilson, D.W., Wiedmann, M., and Rothman, J.E. (1992). Soluble N-ethylmaleimide-sensitive fusion attachment proteins (SNAPs) bind to a multi-SNAP receptor complex in Golgi membranes. J. Biol. Chem. *267*, 12239–12243.

Whiteheart, S.W., Rossnagel, K., Buhrow, S.A., Brunner, M., Jaenicke, R., and Rothman, J.E. (1994). N-ethylmaleimide-sensitive fusion protein: a trimeric ATPase whose hydrolysis of ATP is required for membrane fusion. J. Cell Biol. *126*, 945–954.

Yu, R.C., Hanson, P.I., Jahn, R., and Brunger, A.T. (1998). Structure of the ATP-dependent oligomerization domain of N-ethylmaleimide sensitive factor complexed with ATP. Nat. Struct. Biol. *5*, 803–811.

Zhang, K.Y.J., and Main, P. (1990). Histogram matching as a new density modification technique for phase refinement and extension of protein molecules. Acta Crystallogr. A *46*, 41–46.

Protein Data Bank Accession Number

The accession number for the coordinates of the structure reported in this paper is 1QCS.